Electron cloud density analysis using microwave cavity resonance

2013 JINST 8 P04014

(http://iopscience.iop.org/1748-0221/8/04/P04014)

Operated by Fermi Research Alliance, LLC under Contract No. De-AC02-07CH11359 with the United States Department of Energy.

PUBLISHED BY IOP PUBLISHING FOR SISSA MEDIALAB

RECEIVED: *December 20, 2012*
REVISED: *March 1, 2013*
ACCEPTED: *March 28, 2013*
PUBLISHED: *April 16, 2013*

Electron cloud density analysis using microwave cavity resonance

Y.-M. Shin,[a,b,1] **J.C. Thangaraj,**[b] **C.-Y. Tan**[b] **and R. Zwaska**[b]

[a] *Department of Physics, Northern Illinois University, Dekalb, IL, 60115, U.S.A.*
[b] *Fermi National Accelerator Laboratory, Batavia, IL, U.S.A.*

E-mail: youngmin@fnal.gov

ABSTRACT: We report on a method to detect an electron cloud in proton accelerators through the measurement of the phase shift of microwaves undergoing controlled reflections with an accelerator vacuum vessel. Previous phase shift measurement suffered from interference signals due to uncontrolled reflections from beamline components, leading to an unlocalized region of measurement and indeterminate normalization. The method in this paper introduces controlled reflectors about the area of interest to localize the measurement and allow normalization. This paper describes analyses of the method via theoretical calculations, electromagnetic modeling, and experimental measurements with a bench-top prototype. Dielectric thickness, location and spatial profile were varied and the effect on phase shift is described. The effect of end cap aperture length on phase shift measurement is also reported. A factor of ten enhancement in phase shift is observed at certain frequencies.

KEYWORDS: Accelerator modelling and simulations (multi-particle dynamics; single-particle dynamics); Accelerator Subsystems and Technologies; Beam-line instrumentation (beam position and profile monitors; beam-intensity monitors; bunch length monitors)

[1] Corresponding author.

doi:10.1088/1748-0221/8/04/P04014

2013 JINST 8 P04014

Operated by Fermi Research Alliance, LLC under Contract No. De-AC02-07CH11359 with the United States Department of Energy.

Contents

1 Introduction **1**

2 Theoretical rationale **2**
- 2.1 Analytic model of elliptical beam pipe 2
- 2.2 Main Injector beam pipe cavity 4
- 2.3 Frequency shift from the insertion of a piece of dielectric 4

3 Numerical modelling **5**
- 3.1 Phase shift of microwave traveling through a plasma gas (electron cloud) 5
- 3.2 Dielectric approximation of uniformly distributed electron gas 7
- 3.3 Waveguide and cavity resonator models 9
- 3.4 Electron cloud density calculation 11

4 Parametric analysis **12**

5 Spatial identification of a localized electron gas **12**

6 Experimental test **16**

7 Conclusion **16**

1 Introduction

The electron cloud is caused by the formation of a cloud of non-relativistic electrons in the vacuum chamber of an accelerator. The cloud is seeded through a variety of phenomena, and amplified through acceleration in the electromagnetic field of the beam and secondary emission from the vacuum chamber materials. If the amplification is sufficient, the electron cloud can cause a beam instability by interacting through electrostatic forces with a stored proton (or positron) beam. This instability is a particular concern for the proposed Project X [1], a multi-megawatt proton facility planned for construction at Fermilab. Project X will involve more than tripling the bunch intensity in the Main Injector (MI). The MI is a synchrotron that accelerates 53 MHz proton bunches from 8 GeV to 120–150 GeV. The electron cloud can be seeded in the MI either by residual gas ionization or beam loss on the vacuum chambers. The seed electrons are accelerated transversely by the electric potential of the proton bunches and are amplified upon subsequent collision with the vacuum chamber. The instability can limit the performance of the accelerator by increasing the vacuum pressure, inducing large coherent oscillations, emittance growth, and shifting the tune of the machine, among other things.

Fermilab initiated a program of investigation of the electron cloud to understand the issues concerning an upgrade MI and other high-intensity proton accelerators. One component of this

2013 JINST 8 P04014

program is to develop instrumentation for measuring the formation of the electron cloud. The electron cloud density can be measured by sending EM waves through an electron cloud of uniform distribution and measuring the phase shift of the EM waves [2]. The phase shift of an electromagnetic wave (of frequency, ω) through a uniform, cold plasma (of plasma frequency ω_p and density ρ) per unit length is given by:

$$\frac{\Delta\varphi}{L} = \frac{\omega_p^2}{2c\sqrt{\omega^2 - \omega_c^2}}; \quad \omega_p^2 = 4\pi\rho r_e c^2 \tag{1.1}$$

where c is the speed of light, r_e is the classical electron radius, and ω_c is the cut-off frequency of the pipe. The above formula assumes that the e-cloud density is static but in the MI and other machines, the e-cloud density varies as a function of time because the proton beam which generates the electron cloud has a time pattern of a bunch structure. Therefore, sending a carrier wave into the cloud results in phase-modulation, which can be measured at a receiver some distance from the transmitter. In other words, sidebands to the carrier appear in a frequency spectrum.

By measuring the amplitude of the sideband, in theory, we can estimate the electron cloud density. However, this approach has limitations because the carrier follows many separate paths from the transmitter to the receiver. In general, the carrier will travel in all available directions from the transmitter and reflect from numerous other parts of the machine. These many multiples paths combine at the receiver and result in a measurement that is representative of a much larger region than intended and is generally amplified by the much longer paths. A previous test of an isolated region, surrounded by ferrite absorbers, resulted in phase shifts that were so small as to be nearly immeasurable [3]. Therefore, we need a technique that is localized and yet gives a strong phase-shift. Other technique that are currently used to measure the e-cloud density based on the microwaves includes TE wave resonances and TE wave modulation [4, 5].

Our aim in this work is to make the measurement both localized and increase the signal amplitude. We achieve this by installing reflectors on the beam pipe on either side of the region under study. By deliberately installing reflectors, the reflections are controlled and thereby increase the signal and localize it simultaneously. This paper reports our experimental study of microwave reflection for the specific case of the Fermilab MI beam pipe for various dielectric thickness, orientation and location for different sets of antennae. We begin by describing the experimental setup and then discuss the experimental methods we undertake using simulations and analytic calculations. Next, we discuss the results of the measurement from a bench-top prototype and some ideas for future work.

2 Theoretical rationale

2.1 Analytic model of elliptical beam pipe

The cross section of an MI beam-pipe is approximately elliptic and so it is obvious that we need to go to an elliptic coordinate system to solve for the fields and resonances. The relationship between

2013 JINST 8 P04014

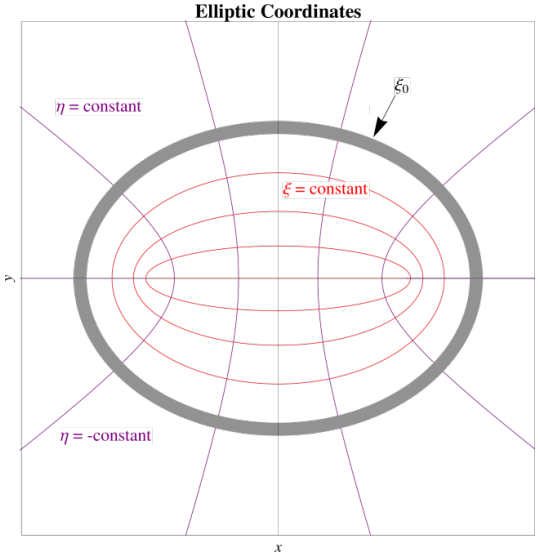

Figure 1. The elliptic coordinate system with lines of constant $\xi > 0$ and $-\pi < \eta \leq \pi$. The transverse cross-sectional wall of the elliptic cavity is at ξ_0.

Cartesian (x, y, z) and elliptic (ξ, η, z) coordinates is

$$x = h\cosh\xi\cos\eta \tag{2.1}$$

$$y = h\sinh\xi\sin\eta \tag{2.2}$$

$$z = z\,. \tag{2.3}$$

Where $h = \sqrt{r_M^2 - r_m^2}$ is the half distance between the foci and lines of constant $\xi > 0$ are ellipses and lines of constant $-\pi < \eta \leq \pi$ are hyperbolae (figure 1). In this case, the wall of the beam pipe is at $\xi = \xi_0$. The resonant modes of an elliptic cavity has been derived elsewhere [4–6] and we will just quote the results here. The resonant frequency of eigenmode (m, n, p) of an elliptic cavity is given by

$$f_m = \frac{c}{2\pi}\sqrt{\frac{4q_{mn}}{h^2} + \left(\frac{p\pi}{d}\right)^2} \tag{2.4}$$

where q_{mn} is defined below, p is the eigenvalue in the longitudinal direction, h is half the distance between the two foci of the ellipse, d is the longitudinal length of the cavity and c is the speed of light in vacuum.

To define q_{mn}, we have to first define the cosine like Mathieu function $\mathrm{Ce}(a, q, z)$[1] which is a solution of the Mathieu equation with characteristic value a and parameter q

$$w'' - (a - 2q\cosh 2z)\,w = 0\,. \tag{2.5}$$

We note that the characteristic value a is a function of the characteristic exponent r and parameter q, i.e. $a \equiv a(r,q)$.[2] For TM modes, q_{mn} is the nth zero of $Ce[a(m,q), \xi_0, z]$, where ξ_0 is the

[1]The argument convention is the same as the *Mathematica* convention for MathieuC. Note: *Ce*(*a*,*q*,*z*) = MathieuC[*a*,*q*,*iz*].

[2]In *Mathematica*, *a*= MathieuCharacteristicA[r,q] for the cosine Mathieu functions.

2013 JINST 8 P04014

elliptic coordinate of the wall of the cavity, $m = 0, 1, 2, \ldots$, and $n = 1, 2, 3 \ldots$. For TE modes, q_{mn} are the zeroes of $Ce\prime[a(m,q), \xi_0, z]$, where "$\prime$" is the derivative w.r.t. z.

2.2 Main Injector beam pipe cavity

We approximate the cross-section of the MI beam pipe with an ellipse and use the dimensions used in the Microwave Studio simulation discussed in section 3.3 for calculating the resonant modes of the cavity. The length of the cavity is $d = 1\,\mathrm{m}$, the length of the semi-major axis is $r_M = 5.9\,\mathrm{cm}$ and the semi-minor axis is $r_m = 2.7\,\mathrm{cm}$. Thus, the half distance between the foci is

$$h = \sqrt{r_M^2 - r_m^2} = 0.052\,\mathrm{m}. \tag{2.6}$$

The elliptic coordinate ξ_0 of the wall of the beam pipe comes from solving

$$\frac{x^2}{\rho^2 \cos^2 \xi} + \frac{y^2}{\rho^2 \sin^2 \xi} = 1 \tag{2.7}$$

for ρ_0 and ξ_0 given the lengths of the semi-major and semi-minor axes, i.e.

$$\rho_0 \cos \xi_0 = r_M \quad \rho_0 \sin \xi_0 = r_m\,. \tag{2.8}$$

Therefore, for the first approximation of the Main Injector beam pipe, we have $\xi_0 = 0.4943\,\mathrm{rad}$. Using these dimensions, we find that the modes between 1.5 GHz to 2.5 GHz are all $\mathrm{TE}_{1,1,,n}$ because the lowest TM mode $\mathrm{TM}_{0,1,0}$ is at 3.3 GHz and $\mathrm{TE}_{0,1,1}$ is at 1.5 GHz.

2.3 Frequency shift from the insertion of a piece of dielectric

The perturbation method for calculating the frequency shift from the insertion of a piece of dielectric into an RF cavity is well-known [9, 10]. Let us suppose that the piece of dielectric is at $z = z_e$ and has thickness Δz_e. See figure 2. This means that both ε and μ behave as follows

$$\varepsilon = \begin{cases} \varepsilon_0 & \text{for } z < z_e \text{ and } z > z_e + \Delta z_e \\ \varepsilon_0 \left(1 + \frac{\Delta\varepsilon}{\varepsilon_0}\right) & \text{for } z_e \le z \le z_e + \Delta z_e \end{cases} \tag{2.9}$$

$$\mu = \begin{cases} \mu_0 & \text{for } z < z_e \text{ and } z > z_e + \Delta z_e \\ \mu_0 \left(1 + \frac{\Delta\mu}{\mu_0}\right) & \text{for } z_e \le z \le z_e + \Delta z_e \end{cases} \tag{2.10}$$

If we assume that $\Delta\varepsilon/\varepsilon_0 \ll 1$ and $\Delta\mu/\mu_0 \ll 1$, so that both the electric fields E and magnetic fields H are approximately equal to the unperturbed fields E_0 and H_0 respectively then we have

$$\frac{\Delta\omega}{\omega_0} = \frac{\int_{\Delta V} d\upsilon \left(\Delta\varepsilon \vec{E}_0^{\,2} - \Delta\mu \vec{H}_0^{\,2}\right)}{\int_{V_c} d\upsilon \left(\varepsilon_0 \vec{E}_0^{\,2} + \mu_0 \vec{H}_0^{\,2}\right)} \tag{2.11}$$

where the integral is over the volume V_c of the cavity, $\Delta\omega = \omega_e - \omega$ and ω_e is the perturbed frequency and ω_0 is the unperturbed resonant frequency. Eq. (2.11) is the result of Slater's perturbation theorem. Therefore, the frequency shift from a small piece of dielectric can be derived if $\vec{E}_0$ and $\vec{H}_0$ are known. In fact, the TM fields of an elliptic cavity have already been derived by Yang [8], and it only takes a little bit of work to get the TE fields. However, since eq. (2.11) has to be numerically integrated anyway, the formula is of academic interest only and will not be used in this paper.

2013 JINST 8 P04014

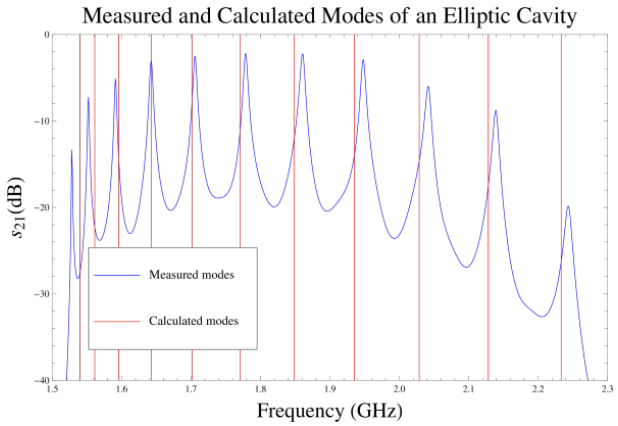

Figure 2. The measured modes using s_{21} and the calculated modes before and after fitting h and d to the measured data from modes $TE_{1,1,4}$ to $TE_{1,1,13}$. The relative difference between the measured and the calculated modes are all $< 1\%$ (see table 1).

Table 1. Elliptic modes of Main Injector cavity.

Mode	Measured	Calculated	Fractional difference (%)
$TE_{1,1,1}$	1.5279	1.5253	-0.17
$TE_{1,1,2}$	1.5522	1.5472	-0.32
$TE_{1,1,3}$	1.5909	1.5832	-0.48
$TE_{1,1,4}$	1.6422	1.6321	-0.62
$TE_{1,1,5}$	1.7052	1.6930	-0.72
$TE_{1,1,6}$	1.7781	1.7646	-0.76
$TE_{1,1,7}$	1.8609	1.8456	-0.82
$TE_{1,1,8}$	1.9482	1.9349	-0.68
$TE_{1,1,9}$	2.0418	2.0314	-0.51
$TE_{1,1,10}$	2.1390	2.1340	-0.23

3 Numerical modelling

3.1 Phase shift of microwave traveling through a plasma gas (electron cloud)

In the experiment, a microwave signal is fed into the pipe through the probe of the coaxial coupler at one side of the pipe and detected by the 2^{nd} probe at the other side. In the simulation, they are modeled with discrete ports, as shown in figure 4. The entire system configuration has been simplified to be the elliptical beam pipe blocked by the apertures that induce signal reflections at both sides of the pipe. In electron gas diagnostics, the phase of a carrier signal, while traveling along the beam pipe, is shifted by the presence of the electron cloud with gas density, n, which is given by

$$\frac{\Delta\varphi}{L} = \frac{\omega_p^2}{2c\sqrt{\omega^2 - \omega_c^2}}, \tag{3.1}$$

2013 JINST 8 P04014

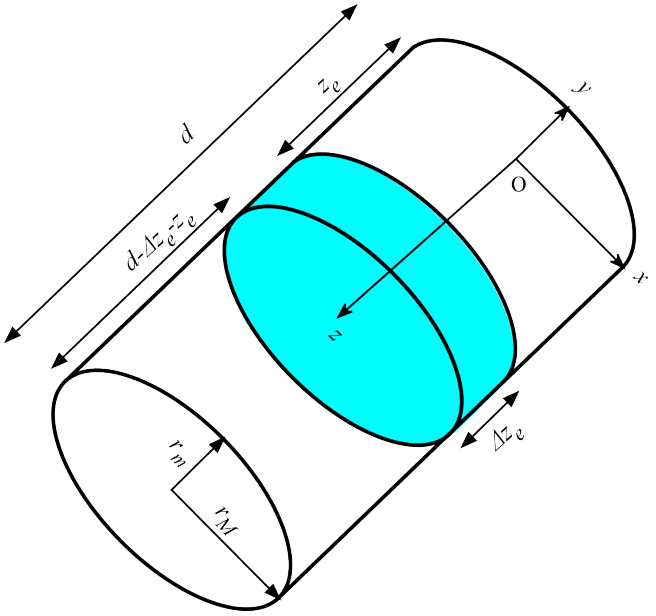

Figure 3. An x-ray view of the elliptical pipe resonator where a dielectric (shaded in cyan) with length Δz_e has been inserted at $z = z_e$.

and

$$\omega_p = \sqrt{\frac{n_e e^2}{\varepsilon_0 m_e}} \cong 56.4\sqrt{n_e} \tag{3.2}$$

where e is the electron charge, ε_0 is the permittivity in free space, and m_e is the electron mass. Electron clouds energized by a proton beam are normally very dilute gas; densities range from 10^{11}–$10^{12}\,\mathrm{m}^{-3}$. The phase shift ratio ($\Delta\varphi/L$) of a traveling wave signal in the dilute gas would be too small to be properly identified; even a 10 m long beam pipe may not enhance the phase shift large enough to be clearly measured by a signal detector (antenna) within the phase resolution. Due to the nature of the single path interaction through the waveguide, traveling waves also have nearly zero response to localized gases, which have no variation on their phase shifts. Therefore, this method is also limited in identifying the spatial location of the electron cloud. On the other hand, a cavity resonator captures waves of the spectrum between a waveguide cutoff and a cavity cutoff and the wave of a cavity eigenmode undergoes a large number of round-trips until it reaches a saturation point (RF filling time), which could remarkably increase a phase shift. Figure 4 shows the conceptual drawing of the resonator electron cloud diagnostics. Multiple trips of a trapped eigenmode effectively increases the travel distance, L, which thereby enhances the phase shift, as depicted in eq. (3.1). The feeble phase shift through a dilute plasma gas can be thus rapidly increased far beyond the resolution limit of a signal detector within a very short distance. Besides, since cavity eigenmodes respond more or less sensitively to electron gases depending upon their locations corresponding to trapped waveforms, the technique might be much more efficient for accurately specifying the spatial position and distribution of the electron cloud.

2013 JINST 8 P04014

3.2 Dielectric approximation of uniformly distributed electron gas

Electron Cloud (EC) simulations using Particle-In-Cell Codes (PIC) provide a powerful tool for understanding cloud build up and mitigation techniques, as well as traveling TE microwave diagnostics of electron clouds. However, to explicitly model sidebands induced in TE waves due to electron cloud plasma, one must simulate beam revolution time scales (the cloud modulation time) while still resolving the rf signal. Modeling electron clouds as kinetic particles is time consuming (particle pushes are slow compared to field updates) and numerically noisy over long simulation times (grid heating). One solution is to replace kinetic particles with an equivalent plasma dielectric model [11]. Plasma dielectric models of electron clouds are much faster, and are more stable numerically.

In the given experimental system, the beam pipe is assumed to be filled with an electron gas, with a density (n), produced by a high intensity proton beam. Although density distribution of a real gas state has a spatial dependence, $n = n(\mathrm{r})$, for simplicity, we first consider a constant density, $n = n_0$. A plasma gas with a constant density can be thus simply approximated as a dielectric medium by a Drude model, as follows.

$$n = \sqrt{\varepsilon \mu}\,, \tag{3.3}$$

where

$$\varepsilon(\omega) = \varepsilon_0 \left(1 - \frac{\omega_p^2}{\omega^2}\right) \quad \text{and} \quad \mu = \mu_0 \tag{3.4}$$

This dielectric approximation very effectively reflects the typical response of a uniformly distributed plasma gas since the gas strongly resonates with an incident wave as ω approaches ω_p. Therefore, the electron cloud could be equivalently modeled with a dielectric medium with an effective dielectric constant, n.

Figure 4 shows a signal processing algorithm from a microwave simulation to calculate a phase shift by an effective electron gas. The port-1 (source) generates a carrier signal of sinusoidal waveform, $S_1(t) = A_1 \sin(\omega\mathrm{t} + \varphi_1)$, where φ_1 is the initial phase ($\varphi_1 = 0$), that travels through the uniformly filled elliptical beam pipe. The detected signal at port-2 (antenna receiver) has the sinusoidal waveform of $S_2(t) = A_2 \sin(\omega\mathrm{t} + \varphi_2 \varphi_m)$, where φ_2 is the initial phase and φ_m is the phase change over the source-to-antenna distance with a dielectric constant, n. In order to extract a phase change, φ_m, from the simulation, let us multiply S_1 and S_2,

$$S_1 S_2 = A_1 A_2 \sin(\omega_1 t) \sin(\omega_2 t + \varphi_m)\,. \tag{3.5}$$

By trigonometric identity, eq. (2.5) becomes

$$S_1 S_2 = \frac{A_1 A_2}{2} \left[\cos(\varphi_m) - \cos(2\omega t + \varphi_m)\right] \tag{3.6}$$

where $\omega = \omega_1 = \omega_2$.

The second term in eq. (3.6), $\cos(2\omega\mathrm{t} + \varphi_m)$, can be removed by a low pass filter (LPF) of a post-processor. The low pass filter process is precisely shown in figure 4. The $S_1 S_2$, obtained from field data monitored at the port-1 and –port2 in simulation, is decomposed into amplitude- and phase-spectra by fast Fourier transform (FFT). The 2^{nd} frequency harmonic term (2ωt) is then

2013 JINST 8 P04014

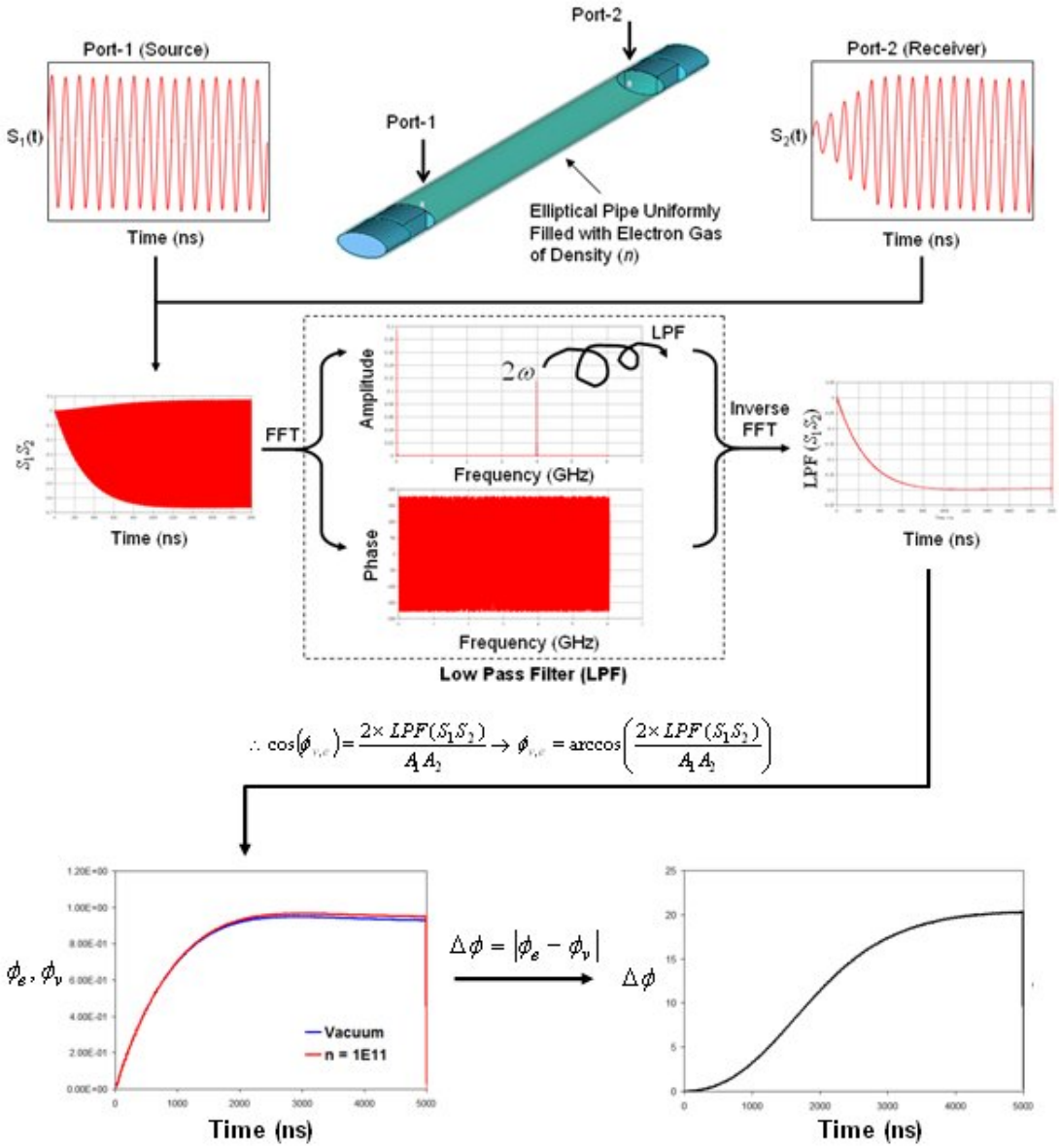

Figure 4. Conceptual flowchart of signal processing and computational algorithm to calculate phase-shifts due to electron clouds from equivalent dielectric simulation models.

crossed out by low pass filtering. The inverse FFT of the LPF'ed amplitude and phase leaves only the cosine term of phase change. Therefore, the phase change, φ_m, is

$$\varphi_m = \cos^{-1}\left(\frac{2\times LPF(S_1S_2)}{A_1A_2}\right) \tag{3.7}$$

The phase shift, $\Delta\varphi$, by an electron cloud is $\Delta\varphi = |\varphi_e - \varphi_v|$, where φ_e is the phase variation (φ_m) through the electron gas and φ_v is the phase variation (φ_m) through a vacuum filled in the beam pipe. This approximation is generally valid since A_1 is constant and A_2 is very slowly varying amplitude, which is nearly constant, in the time scale of signal frequency. Normally, in the simulation A_1 can be set to be a unity, so that A_2 would need to be measured at a time of saturation ($t = t_{\text{saturation}}$).

2013 JINST 8 P04014

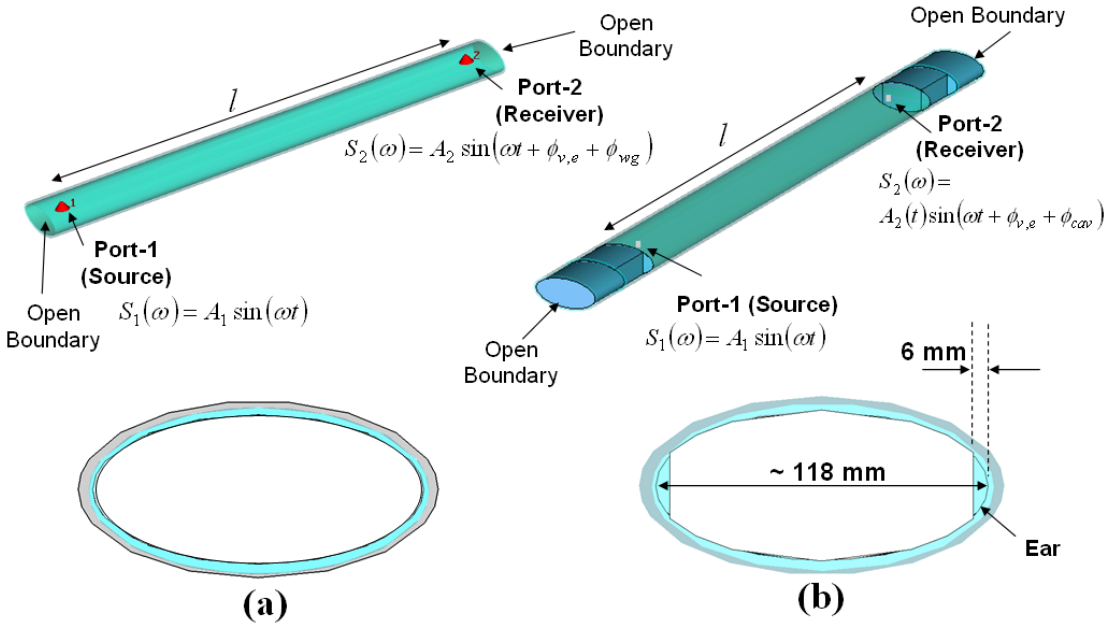

Figure 5. Finite-integral-technique (FIT) simulation models (a) elliptical waveguide and (b) elliptical cavity. Two discrete antenna ports for transmitting and receiving a carrier signal are located adjacent to the open boundaries in the beam pipe. The boundaries are programmed to meet perfect matching layers (PML). The pipe material is designed with a stainless steel.

3.3 Waveguide and cavity resonator models

Applying the same analytic method, we compare the phase shifts of a traveling wave through waveguide and standing wave in a cavity resonator. Figure 5 shows the simulation models based on the elliptical beam pipe: one has ears at both ends to trap waves propagating above the cutoff in the beam pipe, whereas the other is connected only with the open boundary. The pipe length is set to be 1 m and port-to-port distance (l) is 0.95 m. The upper cutoff frequency is determined by the width of the aperture (gap spacing between the ears), which also determine the number of eigenmodes captured in the cavity. The cross-sectional dimensions of the elliptical beam pipe are 11.8 cm (major) $\times$ 5.4 cm (minor), which corresponds to 1.516 GHz of beam pipe cutoff frequency (f_c). The model for the initial numerical analyses was designed to have 6 mm wide ears. Subsequently, however, the ears were re-designed to be 20 mm wide to examine the effect of leakage fields through the apertures since it was found that the beam apertures could be allowed to open up to 80 mm for the proton beam.

As shown in figure 6, the 6 mm wide ear captures 3 resonating modes, (1) 1.5224 GHz (p = 1), (2) 1.5416 GHz (p = 2), and (3) 1.573 GHz (p = 3), between the two cutoff frequencies of the beam pipe and the aperture, 1.516 GHz and 1.974 GHz. The discrepancy between the measured and theoretical frequencies listed in table 1 is attributed to the following reasons: the MI beam pipe is only approximately elliptical in cross section because it was made by squashing a circular beam pipe. Also, the theoretical model is for a closed cavity, whereas the simulated one is based on open boundaries (apertures). Figure 6(b) shows field distributions of those eigenmodes with longitudinal phase changes of p = 1, 2 and 3. Note that the opening size of the apertures is comparable to

2013 JINST 8 P04014

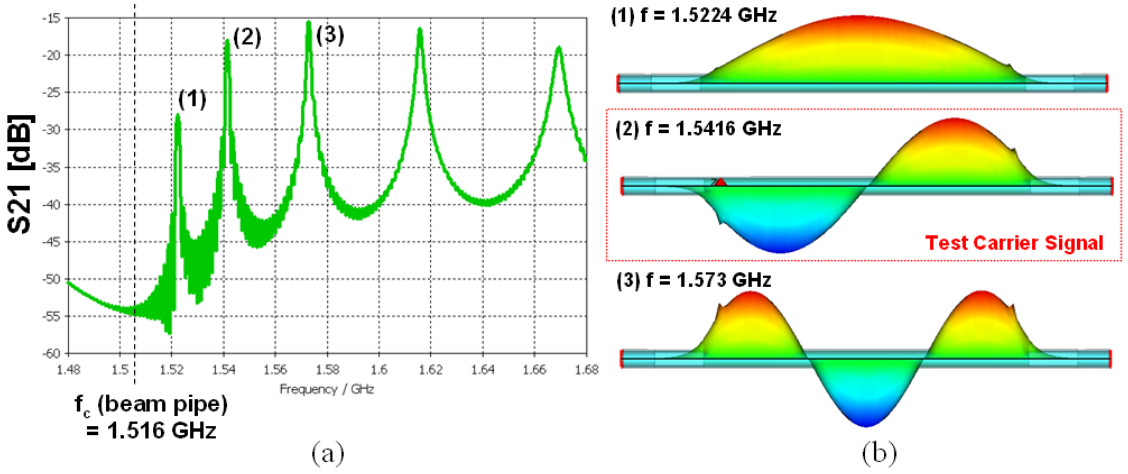

Figure 6. (a) S_{21} spectrum measured at port-1 and -2. The designed beam pipe holds three resonating modes inside (b) field distributions of the three modes (π-mode of $f = 1.5304$ GHz is a carrier signal for time-transient analysis.

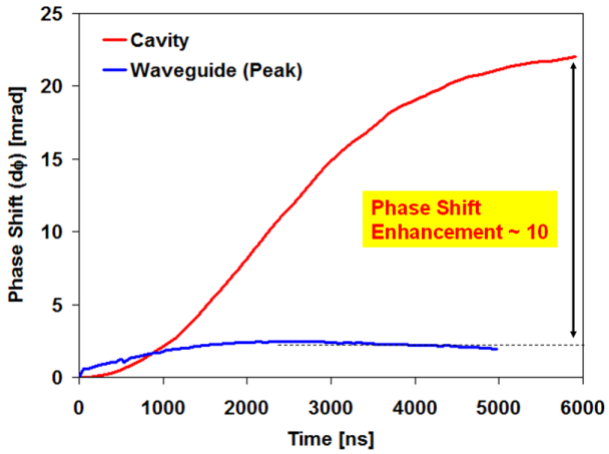

Figure 7. Phase shift versus time graphs of waveguide (blue) and cavity (red) beam pipe models. The cavity enhances the phase-shift by a factor of 10. (ear length/width = 60 mm/6 mm)

the wavelengths, leading to a large leakage of fringe fields. Since the 3π mode (1.573 GHz) has a maximum field amplitude at the aperture position ($z = l/2$), a huge amount of fringe fields is leaked out through the apertures. On the other hand, as depicted in figure 6(b), as the π-mode (1.5224 GHz) has a minimum field amplitude at the cavity fringes, thereby leading to a significantly smaller amount of leakage fields. One can thus see that the π-mode would have a larger phase-shift than the 3π-mode, as shown in eq. (3.1). We choose 2π-mode ($p = 2$, 1.5416 GHz) to compare the phase shift of the cavity with that of the waveguide as the mode properly reflects the average phase shift of the π- and 3π-modes.

Figure 7 shows the phase-shift versus time graphs of the cavity and waveguide models with the 2π-mode carrier ($f = 1.5416$ GHz), which was obtained from the numerical analysis depicted in 2.2. For consistency, the models are simulated with the same condition, e.g., charge density, $n_e =$

2013 JINST 8 P04014

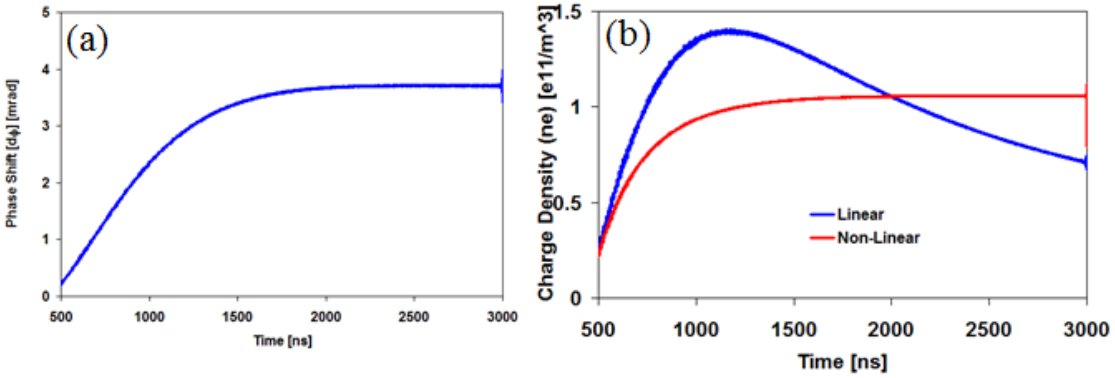

Figure 8. (a) Phase shift versus time graph (b) electron cloud charge density versus time graphs from two different assumptions on the wave traveling distance in the cavity: linear- (blue) and non-linear (red) increases.

10^{11} m^3. The comparative analysis result ended up showing a noticeable improvement: phase shift seems to be enhanced 10 times more by the cavity than the waveguide. In figure 7, the carrier signal in the waveguide quickly reaches the maximum phase shift ($\Delta\varphi \sim 2.3$ mrad) at $t = 2\,\mu$s. However, it continuously rises in the cavity beam pipe up to $\Delta\varphi \sim 23$ mrad until $t = 6\,\mu$s when the cavity reaches a steady state. Ohmic losses and external coupling mainly constrain RF filling time in the cavity that determines the number of round trips (signal travel distance) required to reach a steady state. A phase shift can be thus further increased with a cutoff-nearest mode ($p = 1$: fundamental longitudinal mode), a high conductivity material and a smaller aperture on the beam pipe.

3.4 Electron cloud density calculation

In order to verify the proposed concept of the cavity resonator, we re-calculate the electron cloud density from the cavity-enhanced phase shift of the simulation model. In principle, as a phase shift increases with travel distance, a normalized phase shift should be the same with the same gas density at the steady state either in a cavity or in a waveguide: in eq. (3.1), gas density is the function only of carrier frequency, cutoff frequency, and normalized phase shift, which has no dependence on the distance (L). We first assume that the travel distance linearly increases with time: L is assumed to be proportional to group velocity multiplied by time, $L = v_g \cdot t$. The group velocity is obtained by calculating a time-dependent signal profile. Figure 8 shows the time-dependent charge density graph. The input parameters for the density calculation are given as the 2π-mode carrier frequency of $f = 1.5416$ GHz, $f_c = 1.516$ GHz, and $n_e = 10^{11}$ m^{-3}. The charge density linearly increases until $t = \sim 2\,\mu$s and gradually decreases after the stationary state since the travel distance of the carrier signal is assigned to continuously increase in the definition, whereas the phase shift is saturated after RF filling time. In other words, the phase shift is no longer increased in the time period after a carrier signal of a cycle completely leaves from the resonator, even if L is assumed to continue to increase in the analytic model. Figure 8(b) shows that the charge density at $\sim 2\,\mu$s, corresponding to the saturation time of phase shift in figure 8(a), is $\sim 10^{11}$ m^{-3}, which is exactly matched with the theoretically pre-assigned density to the dielectric Drude model of eqs. (3.3) and (3.4): one can see that the theoretical calculation based on the signal mixing

2013 JINST 8 P04014

technique accurately predicts the electron cloud density, represented with an equivalent dielectric model, in the cavity beam pipe. In order to compensate for the saturation effect, we nevertheless modify the definition of the signal travel distance from a linear increment to one fitting the phase-shift curve in figure 8(a) to more accurately reflects the time-dependent pattern of charge density. The red curve in figure 8(b) is the corrected charge density versus time graph, which clearly shows that the analytic curve converges to the defined density (10^{11} m^{-3}). In this model, the incremental rate of signal travel distance also gradually decreases with that of the phase shift. This calculation technique can thus provide an exact charge density after the simulation time of phase saturation. The comparative analysis verified that a cloud density can be still accurately calculated even from the enhanced phase-shift resolution of the cavity resonance diagnostics.

4 Parametric analysis

In principle, phase-shift enhancement of the cavity beam pipe is mainly determined by the amount of evanescent fringe fields through the apertures. It is understood that the smaller leakage fields lead to the larger phase-shift enhancement over the longer saturation time as a trapped wave has a longer traveling time and distance with smaller external coupling losses. Basically, the phase-shift is thus proportional to a cavity external Q (Q_{ext}). With respect to geometrical configuration of an opened cavity resonator, the amount of leakage fields through the coupling hole-apertures can be reduced by increasing the aperture length to increase Q_{ext} with a fixed width. However, the actual electron cloud diagnostics apparatus in MI ring has the physical constraint to have long ears, so we investigated enhancement factors in terms of the ear length using our theoretical analysis. Figure 9 shows phase-shift graphs in terms of the ear lengths that are calculated with the fixed ear width (= 20 mm) in figure 5(b). The width of the beam pipe aperture was chosen to be $\sim$ 80 mm with the consideration of the maximum proton beam diameter. Sweeping the ear lengths ranges from 25 mm to 150 mm with a 25 mm step. The phase-shift graphs in time domain clearly depicts that the shortest aperture with the longest penetration depth of an evanescent leakage field has the smallest phase-shift resolution with the short saturation time. The converging shift resolution is gradually increased from 8 mrad to 40 mrad as the saturation time moves from $\sim 2\,\mu$s to $\sim 8\,\mu$s, but it does not increase above the ear length = 125 mm as shown in figure 9(b). The beam pipe apertures with $\geq$ 100 mm lengths appear to have significantly small amounts of external energy losses, which thereby need a few thousand round trips for a π-mode standing wave to be completely coupled out with the 1 m long beam pipe cavity. As shown in figure 9(b), the saturated phase-shifts do not exceed $\sim$ 40 mrad as fringe fields at the apertures have a constant amount of leakage with the ear length of $\geq$ 100 mm. However, weakening the leakage fields is constrained by the aperture size, which is thereafter limited due to proton beam size.

5 Spatial identification of a localized electron gas

During its operation, the MI may experience irregular electron gas emissions from the proton beam owing to various unknown factors under the periodic magnetic confinement. Accurate diagnostics of spatiotemporal profiles of this un-controlled localization is one of the critical issues to be resolved. The standing wave characteristic of the resonating cavity technique may be capable of

2013 JINST 8 P04014

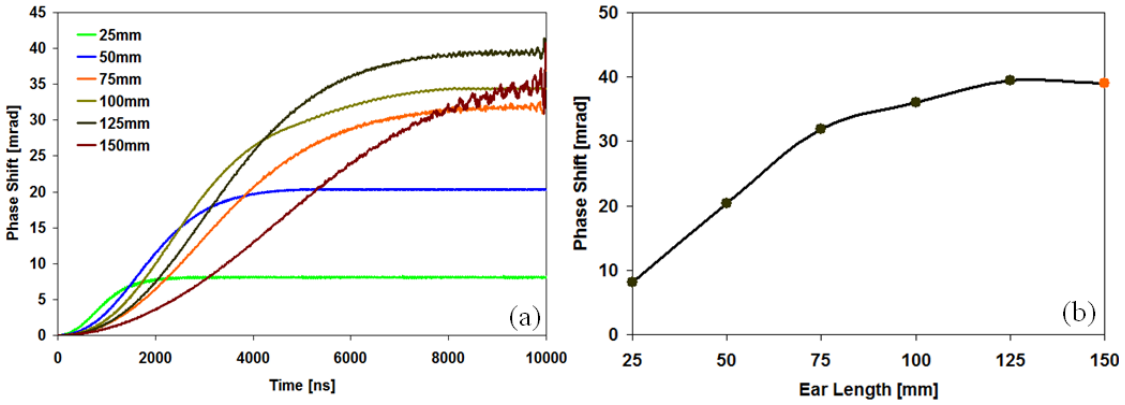

Figure 9. (a) Phase versus time graphs with respect to the ear lengths (b) saturated phase-shift versus ear-length graph (carrier signal: $f = 1.5224$ GHz, π-mode in figure 3(b)). $z = 150$ mm (red) is not fully saturated in $t = 10\,\mu$s.

providing spatial analysis of electron cloud density distribution. It is evident that a phase shift vastly changes depending upon whether the localized electron gas is positioned at a node or an anti-node of a standing wave: in other words, phase change of a carrier signal is maximum with anti-nodes and minimum with nodes. Therefore, phase analysis of multiple carrier signals over the spectrum of resonating modes confined in the beam pipe cavity will make it possible to identify the location and spatial distribution of electron clouds. Figure 7 shows phase-shift spectra ($\Delta\varphi$), between two cutoffs of the beam pipe and aperture, of the two beam pipe fully filled uniform gas and with localized gas, modeled with the 5 cm long dielectric block, and field (E_y) plots corresponding to individual resonating peaks. The dielectric constant of dielectric insertions is defined as ne = 10^{11} m^{-3} electron density. In order to clearly form a standing wave in the simulation, the aperture is designed with a very small width (5 mm) that traps a large number of resonating modes in the beam pipe. In figure 10(a), the maximum field positions of the peaks on the localized gas spectrum are all exactly matched with the dielectric position of z = 0 m. The other non-resonating peaks disappear. With z = 0.125 m, 0.25 m and 0.375 m in figures 10(b)–(d), one can see that the peaks with anti-nodes closely matched with the dielectric positions remain on the localized gas spectrum whereas the other peaks with nodes matched with the positions appear to have nearly zero phase shift, which thereby disappear in the spectra. Note that the lower frequency modes have larger phase shifts with smaller spatial resolution, while higher frequency signals have better spatial resolution as phase shift becomes smaller with an increase of frequency. As the phase shift is also proportional to a traveling distance, a localized gas thickness would thus need to exceed a certain value to have distinct resonating peaks in the high frequency spectrum. However, overlapping the field distributions of resonating modes will enable one to accurately conjecture a position of electron gas, including mapping a one-dimensional density distribution. Although these simulation results verify the diagnostic method of microwave resonant cavity, more systematic investigation is still necessary to explore its feasibility for the spatial and temporal electron cloud mapping and is currently under development.

2013 JINST 8 P04014

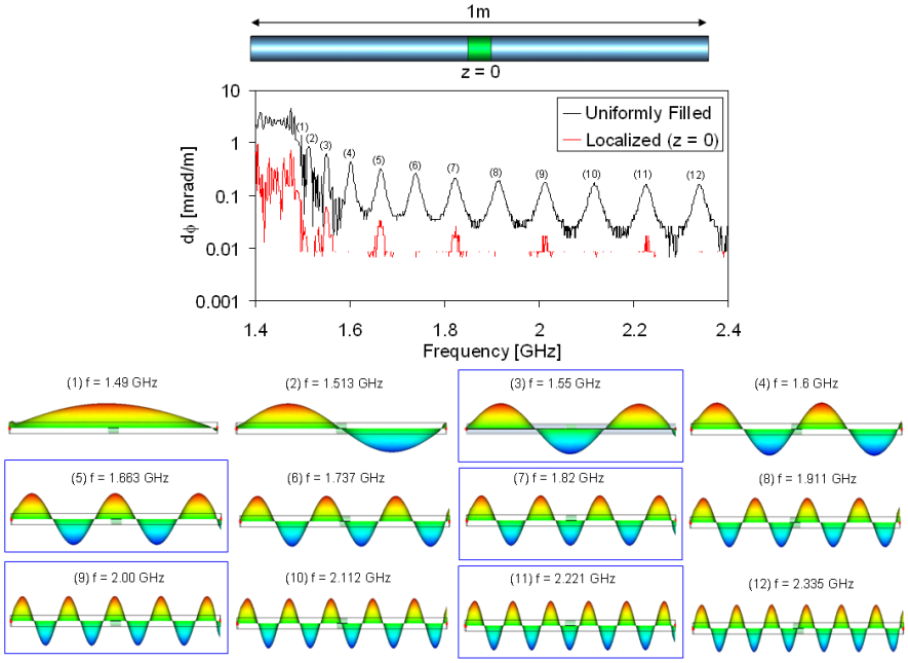

(a)

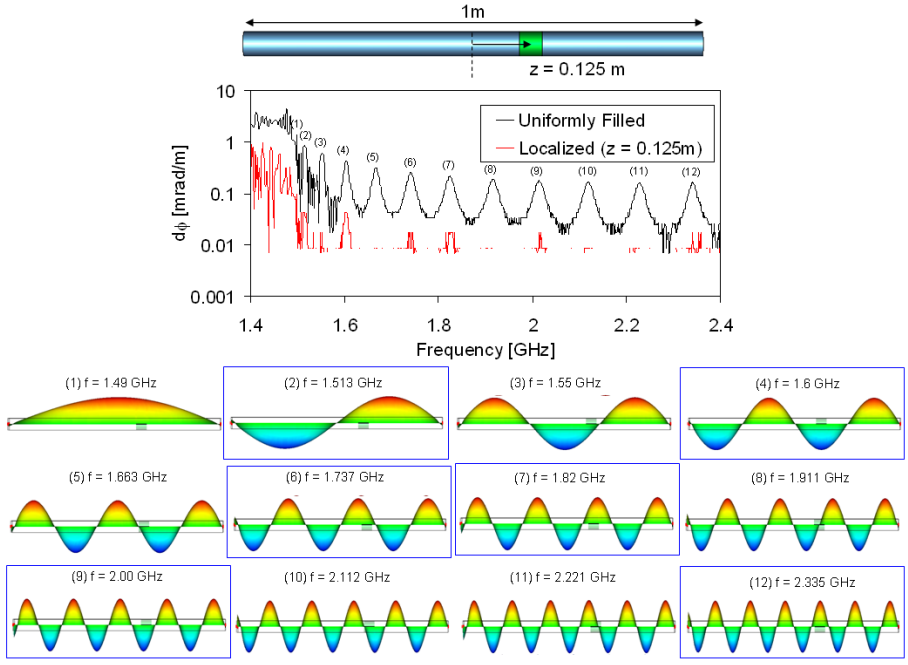

(b)

2013 JINST 8 P04014

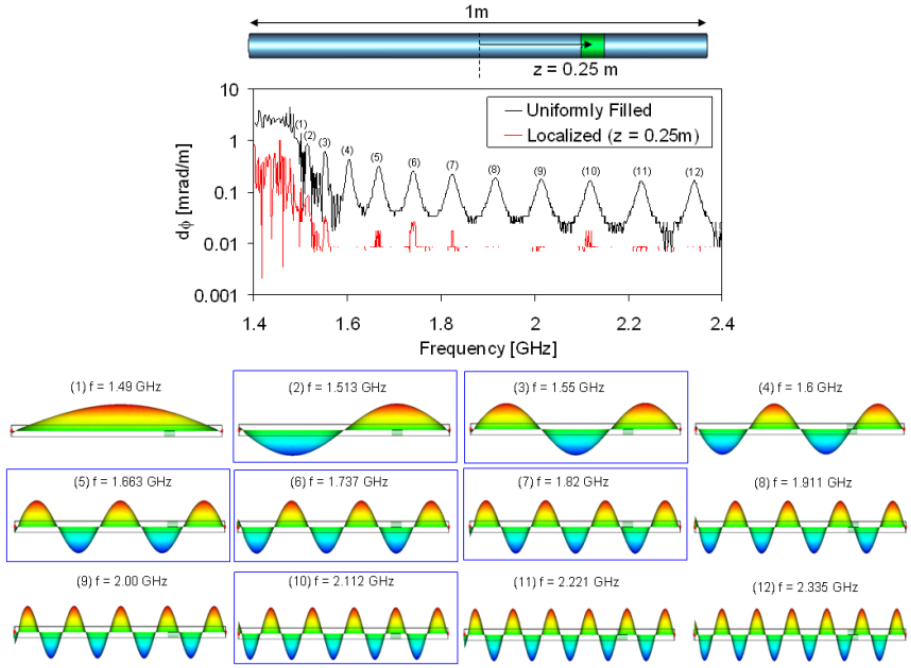

(c)

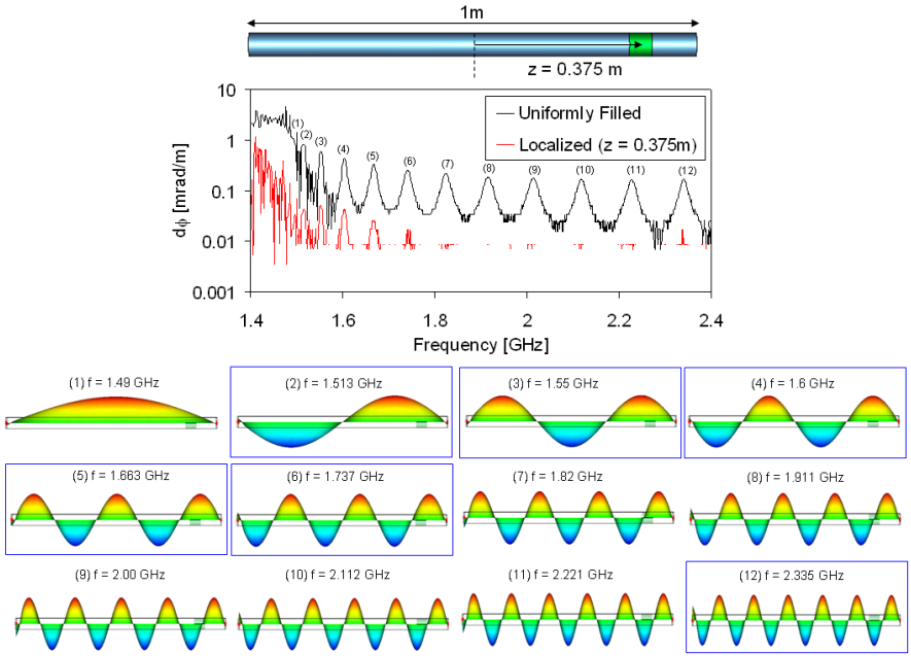

(d)

Figure 10. Phase shift spectra and eigenmode field plots of localized electron clouds with respect to the axial positions of the equivalent model (electric insertion): (a) z = 0 m (b) z = 0.125 m (b) $z = 0.25$ m, and (d) z = 0.375 m.

2013 JINST 8 P04014

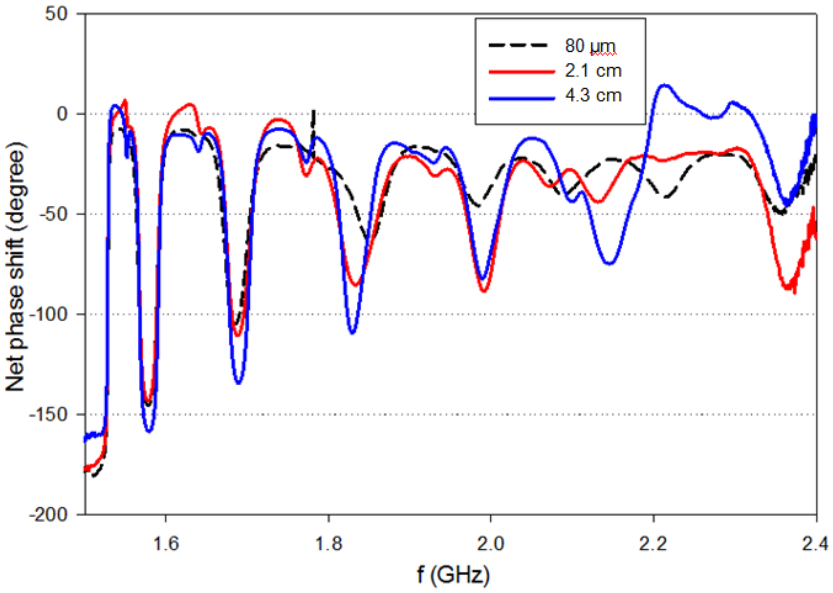

Figure 11. Phase shift due to 2.7 cm thick dielectric at the center of the new setup for 8.26 cm aperture width. The graph compares phase shift for three different thicknesses: 80 μm (negligible thickness), 2.1 cm and 4.3 cm. The phase signal is generally larger for thicker reflector.

6 Experimental test

In order to test the effectiveness of the reflector 'ears', we performed a series of bench-top experiment with the MI pipe of 1 m length and a cross section 11.8 cm by 5.4 cm. We set up the network analyzer to generate microwave signal with a frequency span from 1.5 GHz to 2.4 GHz with a bandwidth of 10 kHz, and measure the phase of S_{21} transmission. Two 5.08 cm half-wave dipoles in transverse orientation are used to transmit and receive even TE_{11} mode with cutoff frequency at around 1.516 GHz. To model the e-cloud, we placed the 2.7 cm dielectric (Teflon) at the center of the waveguide. The phase data were collected with and without the dielectric inside the waveguide. We calculated the phase shift of the signal due to the dielectric by subtracting the phase data without the dielectric from the phase data with the dielectric. Reflectors of three different thickness, 80 μm, 2.1 cm, and 4.3 cm, were designed. The aperture was set to 108 mm as mentioned in figure 5(b). Figure 11 shows the phase-shift due to three different reflector thicknesses. As predicted by the simulation, the thicker the reflector-ears, the higher the phase-shift. A separate experiment using distributed dielectric also indicates phase-shift improvement when thick ears are used as reflectors.

7 Conclusion

We have developed an effective method to accurately measure the density of dilute electron clouds generated by high intensity proton beams. The strong phase shift enhancement from multiple reflections of standing waves in a resonating beam pipe cavity has been demonstrated with numerical modeling using dielectric approximation and microwave S-parameter measurements. The equivalent dielectric simulation showed a $\sim$ 10 times phase shift enhancement (2π-mode, 1.5416 GHz)

2013 JINST 8 P04014

with the cavity beam pipe compared to the waveguide model. The position-dependence of the technique is investigated by overlapping the field distributions of harmonic resonances. The simulation with various positions of dielectric insertions confirmed that resonance peaks in phase-shift spectra corresponding to the relative distance between field-nodes and electron cloud position, which allows for one-dimensional mapping. Preliminary experimental studies based on a bench-top setup confirm the simulation showing that thicker reflectors enhance the phase-shift measurement of the electron cloud density.

Acknowledgments

We would like to acknowledge B. Fellenz for the support of the experiment. We also thank the Lee Teng interns Hexuan Wang and Phyo Kyaw for the experimental work on the prototype.

References

[1] S. Nagaitsev, *Project X - New Multi Megawatt Proton Source at Fermilab*, at *PAC'2011 conference*, New York U.S.A. (2011), FROBN3.

[2] S. De Santis et al., *Measurements of the Electron Cloud in Large Accelerators By Microwave Dispersion*, *Phys. Rev. Lett.* **100** (2008) 094801.

[3] R. Zwaska, *Electron cloud experiments at Fermilab: formation and mitigation*, *Conf. Proc.* **C110328** (2011) 27, PAC-2011-MOOBS4, FERMILAB-CONF-11-081-APC.

[4] S.De Santis et al., *Analysis of Resonant TE Wave Modulation Signals for Electron Cloud Measurements*, in *Proceedings of International Particle Accelerator Conference 2012*, New Orleans U.S.A. (2012).

[5] J.P. Sikora et al., *Using TE Wave resonances for the Measurement of electron cloud density*, in *Proceedings of International Particle Accelerator Conference 2012*, New Orleans U.S.A. (2012).

[6] A. Pietropaolo et al., *DINS measurements on VESUVIO in the resonance detector configuration: proton mean kinetic energy in water*, 2006 *JINST* **1** P04001.

[7] A.I. Harris, *Spectroscopy with multichannel correlation radiometers*, *Rev. Sci. Instrum.* **76** (2005) 054503 [astro-ph/0504449].

[8] G.F. Knoll, *Radiation detection and measurements*, John Willey and Sons Inc., New York U.S.A. (2000).

[9] L.C. Maier and J.C. Slater, *Field Strength Measurements in Resonant Cavities*, *J. Appl. Phys.* **23** (1952) 68.

[10] L.B. Mullet, G/R.853, Atomic Energy Research Establishment, Harwell U.K. (1952).

[11] S.A. Veitzer, D.N. Smithe and P.H. Stoltz, *Application of new simulation algorithms for modeling rf diagnostics of electron clouds*, *AIP Conf. Proc.* **1507** (2012) 404.

2013 JINST 8 P04014